TITLE: Epidermal Growth Factor Receptor Regulates Beclin-1 in Hyperoxia

AUTHORS: Zachary M. Harris MD[1,2]; Asawari Korde PhD[2]; Johad Khoury MD[2]; Edward P. Manning[1,2]; Gail Stanley MD[1]; Ying Sun MD[2]; Buqu Hu MS[2]; Hyeon Jun Shin PhD[2]; John Joerns MD[3]; Brian Clark MD[1,2]; Lindsey Placek[4]; Derya Unutmaz MD[4]; Hyung Chun MD FAHA[5]; Lokesh Sharma PhD[6]; Maor Sauler MD[2]; Govindarajan Rajagopalan BVsc MVSc PhD[2]; Xuchen Zhang MD PhD[7]; He Wang MD PhD[1,7]; Min-Jong Kang MD PhD MPH[2]; Jonathan L. Koff MD[2]

AUTHOR AFFILIATIONS:

1. VA Connecticut Healthcare System, West Haven, Connecticut, United States, 06516
2. Section of Pulmonary, Critical Care, and Sleep Medicine; Department of Internal Medicine; Yale University School of Medicine; New Haven, Connecticut, United States, 06510
3. Division of Pulmonary and Critical Care; Department of Internal Medicine; UT Southwestern Medical Center; Dallas, Texas, United States, 75390
4. The Jackson Laboratory for Genomic Medicine; Farmington, Connecticut, 06032
5. Section of Cardiovascular Medicine; Department of Internal Medicine; Yale University School of Medicine; New Haven, Connecticut, United States, 06510
6. Division of Pulmonary, Allergy, Critical Care, and Sleep Medicine; Department of Medicine; University of Pittsburgh Medical Center; Pittsburgh, Pennsylvania, United States, 15261
7. Department of Pathology; Yale University School of Medicine; New Haven, Connecticut, United States, 06510

ABSTRACT:

Introduction: More than 300,000 patients are placed on mechanical ventilation in the ICU annually in the United States. Many of these patients will require hyperoxia (>70% oxygen) to prevent tissue hypoxia. We have previously shown that the tyrosine kinase receptor epidermal growth factor receptor (EGFR) regulates alveolar epithelial apoptosis in hyperoxia. Mice with reduced total EGFR activity ($EGFR^{Wa5/+}$ mice) show improved survival and reduced markers of ALI compared with WT in hyperoxia. How EGFR regulates additional cell death pathways in hyperoxia remains to be explored.

Methods: We tested the hypothesis that EGFR regulates the molecule coiled-coil moesin-like BCL2-interacting protein (Beclin-1 [BCN1]), which is known to induce autophagy, in hyperoxia. Effects of 100% oxygen were studied in $EGFR^{Wa5/+}$ mice and wildtype (WT) littermates. Mice were exposed to 100% oxygen for 24, 48, and 72 hours and compared with normoxia controls. Lungs were analyzed for BCN1 via Western blot (WB), RT-qPCR, immunohistochemistry (IHC), and flow cytometry. Whole-lung and cell-specific analyses were completed. The specific BCN1 phosphorylation site (p-BCN1), serine residue 91 and 94 (Ser91, -94) for mouse (Ser93, -96 for human), that regulates autophagy was examined.

Results: In WT mice, hyperoxia induced increased whole-lung BCN1 compared with normoxia via WB and RT-qPCR. Whole-lung and epithelial-specific p-BCN1 was increased compared with normoxia via IHC and flow cytometry. Hyperoxia led to increased autophagy via WB and RT-qPCR. $EGFR^{Wa5/+}$ mice showed increased BCN1 and reduced p-/total BCN1 ratios in hyperoxia compared with WT via WB. $EGFR^{Wa5/+}$ mice also showed increased BCN1 via RT-qPCR and decreased epithelial-specific p-/total BCN1 ratios via flow cytometry, although this did not reach statistical significance. $EGFR^{Wa5/+}$ mice showed reduced autophagy via WB compared with WT in hyperoxia.

Conclusions: Hyperoxia induced increased whole-lung and epithelial-specific BCN1 in hyperoxia and resulted in increased autophagy. Decreased EGFR activity, which leads to improved survival in hyperoxia, resulted in decreased whole-lung p-/total BCN1 ratios and decreased epithelial-specific p-/total BCN1 ratios in hyperoxia *in vivo*. Because BCN1 and autophagy can regulate cell death, EGFR regulation of p-BCN1 and autophagy is a mechanism in hyperoxia with therapeutic potential.

INTRODUCTION:

More than 300,000 patients are placed on mechanical ventilation in the intensive care unit (ICU) annually in the United States (1-3). Many of these patients will require very high oxygen (>70%), called *hyperoxia*, during their clinical course (4, 5). Hyperoxia leads to epithelial cell death in the lung (6). Patients receive hyperoxia to treat hypoxic respiratory failure caused by multiple forms of acute lung injury (ALI), such as infectious pneumonia, pulmonary embolism, and acute respiratory distress syndrome (ARDS). Thus, mechanisms of cell death induced by hyperoxia occur concomitantly with those induced by other forms of ALI and by ventilator-induced lung injury (VILI). It is therefore critical to identify mechanisms of cell death caused by hyperoxia to elucidate lung pathobiology for patients with ALI/ARDS who require high oxygen. In addition, ALI induced by hyperoxia is a model for ARDS. Despite the large number of patients hospitalized with ARDS each year and the substantial mortality for this condition (7), there are no medical therapies for ARDS. Thus, elucidation of novel therapeutic targets for ARDS is critical. Identifying therapeutic targets in hyperoxia has translational potential for therapeutic targets in ARDS.

Epidermal growth factor receptor (EGFR) is a receptor tyrosine kinase with pleiotropic cellular effects that, when activated, is involved in multiple cellular processes that are beneficial in ALI. These include alveolar epithelial cell proliferation (8, 9), alveolar epithelial cell migration (8, 10, 11), epithelial cell barrier restoration after injury (12), wound repair in airway (13) and alveolar epithelial cells (11), and respiratory epithelial repair following naphthalene-induced ALI (14, 15). However, EGFR activation has been shown to be deleterious in other contexts in ALI, such as in VILI (16) and lipopolysaccharide (LPS)-induced ALI (17). In addition, EGFR activation can be deleterious in asthma (18), pulmonary fibrosis (19, 20), and viral infection (21-23). We previously showed that inhibition of EGFR is protective in hyperoxia-induced ALI by reducing apoptotic cell death in alveolar epithelial cells (24). In addition, inhibition of EGFR resulted in reduced extracellular signal-regulated kinase 1 and 2 (ERK1/2) activation in the lung and in alveolar epithelial cells. Based on the pleiotropic effects of EGFR, we hypothesized that inhibition of EGFR is beneficial in hyperoxia via additional mechanisms.

Autophagy is a dynamic, homeostatic process wherein stress conditions induce biogenesis of autophagosomes that sequester unwanted contents for recycling (25, 26). While generally considered beneficial (27), the role of autophagy in hyperoxia is not clear (28). Coiled-coil moesin-like BCL2-interacting protein (Beclin-1 [BCN1]) induces autophagy by forming a key signaling complex through highly regulated mechanisms. BCN1 contains a BCL2 homology 3 (BH3) domain, and because B-cell lymphoma 2 (BCL2) molecules contain and signal through BH1-4 domains (29), BCN1 acts as a nexus between apoptosis and autophagy (30). In addition, BCN1 contains distinct phosphorylation sites that, when activated, can either promote or downregulate autophagy (30). EGFR regulates BCN1 in cancer, which affects autophagy (31-33). However, EGFR regulation of BCN1-mediated autophagy has not been studied in hyperoxia. Based on this, we hypothesized that regulation of BCN1 and autophagy is a mechanism whereby EGFR inhibition provides protection in hyperoxia.

In this study, we examined the effects of EGFR inhibition on BCN1 and autophagy in hyperoxia. We found that BCN1 and autophagy are activated in hyperoxia. We found that the increase in BCN1 is localized to the airway epithelium. In addition, we found that genetically altered mice with reduced EGFR activity, which are protected in hyperoxia and have reduced alveolar epithelial apoptosis (24), show decreased BCN1 phosphorylation and reduced autophagy in the lung. We believe that EGFR regulation of BCN1 and autophagy in hyperoxia is a novel mechanism and a potential therapeutic target in ALI that warrants further study.

MATERIALS AND METHODS:

Mice

EGFR-deficient mice containing the Wa5 Egfr allele ($EGFR^{Wa5/+}$ mice) were a generous gift from Dr. David Threadgill at Texas A&M College of Medicine. The Egfr Wa5 allele contains a missense mutation within the EGFR coding region that results in decreased EGFR activity (34). Thus, Egfr Wa5 functions as a hypomorphic Egfr allele. The genetic background of $EGFR^{Wa5/+}$ mice is BALB/c, C3H, and C57Bl/6J (34). Mice were kept and maintained in the Yale Animal Resource Center.

Oxygen Exposure

Adult eight (8)- to ten (10)-week-old mice were exposed to 100% oxygen delivered continuously in a plexiglass hyperoxia chamber (35). For survival experiments, mice (n=6 per group) were closely monitored, and time of death was recorded. For timed exposures, mice (n=6 per group) were exposed to 100% oxygen continuously for 24 hours (mild injury), 48 hours (moderate injury), and 72 hours (severe injury). Lung specimens were taken for RNA, protein, and immunohistochemistry analysis (described below). All protocols were reviewed and approved by Yale University Institutional Animal Care and Use Committee.

Western Blotting

Specific proteins were evaluated and compared using Western blot analysis (36). For whole lung homogenates, lung tissue was homogenized in radioimmunoprecipitation assay (RIPA) buffer (Thermo Fisher Scientific, Waltham, MA, USA; catalog # 89900) and supplemented with protease inhibitor (Roche, Basel, Switzerland; reference # 11836170001) and phosphatase inhibitors sodium orthovanadate (New England Biolabs, Ipswich, MA, USA; item # P0758) and sodium fluoride (New England Biolabs; item # P0759). Western blotting was performed using a sodium dodecyl-sulfate polyacrylamide gel electrophoresis (SDS-PAGE) system (Bio-Rad, Hercules, CA, USA; item # 8658004). Samples were electrophoresed in a 4-20% polyacrylamide gel (Bio-Rad; item # 4568095) in tris-glycine-SDS buffer (Bio-Rad; catalog # 1610772) and transferred to a polyvinylidene fluoride (PVDF) membrane (Bio-Rad; item # 1704157). Samples were subsequently probed with rabbit anti-phospho-Beclin-1 (Ser93, -96) (1:1000 dilution; Thermo Fisher Scientific; catalog # PA5-67514), mouse anti-Beclin-1 (1:1000 dilution; Santa Cruz, Dallas, TX, USA; item # sc-48341), rabbit anti-LC3B (1:1000 dilution; Cell Signaling Technologies, Danvers, MA, USA; item # 2775), and mouse anti-β-Actin (1:1000 dilution; Santa Cruz;

item # sc-47778) primary antibodies overnight at 4˚C. Samples probed with rabbit primary antibodies were subsequently probed with horseradish peroxidase (HRP)-linked anti-rabbit IgG (1:2500 dilution; Cell Signaling Technologies; item # 7074) secondary antibodies. Samples probed with mouse primary antibodies were subsequently probed with HRP-linked anti-mouse IgG (1:2500 dilution; Cell Signaling Technologies; item # 7076) secondary antibodies. Protein band densitometry analysis was completed using ImageJ software.

Reverse Transcription-Quantitative Polymerase Chain Reaction

Fold changes for specific mRNA were evaluated using reverse transcription-quantitative polymerase chain reaction (RT-qPCR) (37). Mouse lungs were collected and homogenized in TRIzol Reagent (Thermo Fisher Scientific, Carlsbad, CA, USA; item # 15596) and homogenized using the Precellys 24 bead mill homogenizer (Bertin Technologies, Montigny-le-Bretonneux, France). RNA was isolated and washed. RNase (Roche, Mannheim, Germany; item # 6011960) and DNAse (Roche; item # 04716728001) were added to the mixture. RNA integrity was confirmed, and RNA quantity was measured using a NanoDrop 2000 microvolume spectrophotometer (Thermo Fisher Scientific, Wilmington, DE, USA; item # ND-2000). 1 µg RNA was synthesized to cDNA by reverse-transcription using the iScript cDNA Synthesis Kit (Bio-Rad, Hercules, CA, USA; item # 1708891). Real-time PCR was performed in 10 µl reactions containing 5 µl SsoFast EvaGreen Supermix with Low ROX (Bio-Rad; item # 1725211) diluted 1:2, 2 µl cDNA template (diluted 1:10), 0.5 µl forward primer, 0.5 µl reverse primer, and 2 µl deionized water. Quantitative PCR was performed with the ViiA 7 Real-Time PCR System (Applied Biosystems, Waltham, MA). Primers for real-time PCR were manufactured at the Keck Biotechnology Research Laboratory at Yale University (New Haven, CT, USA). The following primers were used: BCN1, 5′-CTGAAACTGGACACGAGCTTCAAG-3′ and 5′-CCAGAACAGTATAACGGCAACTCC-3′ (38); BCN1, ′-TTT TCT GGA CTG TGT GCA GC-3′ and 5′-GCT TTT GTC CAC TGC TCC TC-3′ (39); Atg5, 5′-GACAAAGATGTGCTTCGAGATGTG-3′ and 5′-GTAGCTCAGATGCTCGCTCAG-3′ (38); ATG7, 5′-ATGCCAGGACACCCTGTGAACTTC-3′ and 5′-ACATCATTGCAGAAGTAGCAGCCA-3′ (40); LC3a,5′-AGCTTCGCCGACCGCTGTAAG-3′ and 5′-CTTCTCCTGTTCATAGATGTCAGC-3′ (38); and LC3b, 5′-CGGAGCTTTGAACAAAGAGTG-3′ and 5′-TCTCTCACTCTCGTACACTTC-3′ (38). The levels of mRNA were normalized to GAPDH. Fold changes were calculated using the $2^{-\Delta\Delta CT}$ method.

Immunohistochemistry

Mice were anesthetized, the pulmonary intravascular space was cleared, and whole lungs were dissected from mice and immediately placed in 4ºC buffered formalin overnight for paraffin embedding (35). Immunohistochemistry was performed on 5-µm sections by the Yale Histopathology Core. Antigen retrieval was completed in antigen retrieval buffer. Lung sections were labelled with rabbit anti-Beclin-1 (Abcam, Waltham, Massachusetts, USA; catalog # ab62557) antibodies, 1:400 overnight at 4˚C. Subsequently, sections were incubated in anti-rabbit secondary antibodies conjugated to horseradish peroxidase. Slides were analyzed with an Eclipse Ni upright microscope (Nikon, Melville, NY, USA). Images were captured using a DS Ri2 microscope camera (Nikon) with NIS Elements software version 4.30 (Nikon). Cell-specific localization of BCN1-positive cells was determined by two independent observers (Drs. Harris and Zhang). H-scores were calculated for BCN1 by

assigning a staining intensity ordinal value for each cell as follows: 0 for no signal, 1 for mild signal, 2 for moderate signal, and 3 for strong signal (41). The percentage of cells for each staining intensity ordinal value was multiplied by the respective staining intensity ordinal value, and the H-score was calculated by adding the four products together, such that H-score = 0(% cells counted as none) + 1(% cells counted as mild) + 2(% cells counted as moderate) + 3 (% cells counted as strong). An H-score ranging from 0-300 was generated. 100 cells were counted for each sample.

Flow Cytometry

Mouse lungs were analyzed via flow cytometry for whole-lung and epithelial-specific BCN1 (phospho- [p-] and total-). The pulmonary arterial circulation was cleared by perfusing iced-cold saline via the right ventricle. Lungs were isolated, and one half of the right lung was digested by finely cutting the lung into small pieces and passing the pieces through a 70 µm cell strainer (Falcon [Corning], Glendale, AZ, USA; item # 352350) using mechanical force with the back of a syringe. The cells were resuspended in FACS buffer containing 0.5% bovine serum albumin (Sigma Aldrich, St. Louis, MO, USA; item # 9647) in PBS. ACK lysing buffer (Lonza, Walkersville, MD, USA; catalog # 10-548E) was used to lyse red blood cells. After blocking with a monoclonal anti-CD16/32 Fc block solution (Biolegend, San Diego, CA, USA; catalog # 101320; clone 93; lot # B230968), cells were labeled with surface markers using the following antibodies: anti-CD45 monoclonal conjugated to eFluor 450 (Invitrogen, Carlsbad, CA, USA; reference # 48-0451-82; clone 30-F11; lot # 2640501; dilution 1:100), anti-CD31 monoclonal conjugated to phycoerythin (PE) (Invitrogen; reference # 12-0311-81; clone 390; lot # E01191-1634; dilution 1:40), and anti-CD326/EpCAM monoclonal conjugated to allophycocyanin (APC) (Invitrogen; reference # 17-5791-82; clone G8.8; lot # 2565467; dilution 1:100). After surface marker labelling, cells were subsequently fixed using BD Cytofix/Cytoperm solution (BD Biosciences, Franklin Lakes, NJ, USA; catalog # 51-2090KZ). Cells were subsequently permeabilized using BD Perm/Wash buffer (BD Biosciences, Franklin Lakes, NJ, USA; material # 554723), and intracellular labelling was completed. For this, cells were labeled with anti-phospho-BCN1 (Ser93, -96) polyclonal rabbit antibodies (Thermo Fisher Scientific; catalog # PA5-67514; 1:100 dilution, diluted in FACS buffer), washed, and labeled with goat anti-rabbit secondary polyclonal antibodies conjugated to Alexa Fluor 594 (Invitrogen; catalog # A-11012; 5 µg/ml dilution, diluted in FACS buffer). Cells were then washed and subsequently labeled with polyclonal antibodies against total BCN1 conjugated to fluorescein isothiocyanate (FITC) (Bioss, Woburn, MA, USA; catalog # bs-1353R-FITC; lot # A103225367; 1:60 dilution, diluted in FACS buffer). Cells were washed with BD Perm/Wash buffer twice and resuspended in FACS buffer. BCN1 and p-BCN1 positive cells were determined using a BD LSRII flow cytometer within the Yale Flow Cytometry core facility (BD Biosciences, Franklin Lakes, NJ, USA). Flow cytometry data was analyzed using FlowJo software version 10.9.0 (FlowJo LLC [Becton Dickenson], Ashland, Oregon, USA).

Statistical Analysis

Molecular data were examined by analyses of variance to estimate means and standard errors. Statistical significance was assessed by two-tailed *t*-tests and Mann-Whitney tests. Graphs and statistical analyses were completed using GraphPad Prism version 10.1.1 (GraphPad Software version 10.1.1, La Jolla, CA, USA).

RESULTS:

Hyperoxia induces BCN1 phosphorylation and BCN1 production in the lung *in vivo*

Very high oxygen, called *hyperoxia*, has been shown to induce autophagy in mouse lung and human epithelial cells (28). Coiled-coil moesin-like BCL2-interacting protein (Beclin-1 [BCN1]) forms a complex with vacuolar protein sorting 34 (VPS34), vacuolar protein sorting-associated protein 15 (VPS15), and autophagy related 14 (ATG14) which leads to initiation of autophagy. Based on this, effects of 100% oxygen on BCN1 were examined in mouse lungs. Wildtype (WT) mice were exposed to 100% oxygen for 24, 48, and 72 hours, and lungs were analyzed for BCN1. Whole-lung BCN1 (phosphorylated- [p-] and total- fraction) was evaluated via Western blot (Figure 1A-C). Phosphorylation of BCN1 was evaluated for the serine residue 91 and 94 (Ser91, -94) for mouse or Ser93, -96 for human, which leads to activation of the BCN1-VPS34 complex and subsequent initiation of autophagy (42). The ratio of p-/total BCN1 increased at 48 hours of 100% oxygen compared with 24 and 72 hours (Figure 1A-B). The total BCN1/β-Actin ratio increased at 48 hours compared with normoxia and 24 hours of 100% oxygen (Figure 1A, 1C). In addition, whole-lung expression of BCN1 was evaluated via reverse transcription-quantitative polymerase chain reaction (RT-qPCR) (Figure 1D). BCN1 expression increased at 72 hours of 100% oxygen compared with normoxia and 24 hours (Figure 1D). BCN1 expression increased at 48 hours compared with 24 hours (Figure 1D). To confirm these findings, we used a separate RT-qPCR primer for BCN1, and the results were similar that BCN1 expression increased with hyperoxia (Figure S1A in Supplemental Data). In addition, BCN1 in the lung was also evaluated via immunohistochemistry (Figure 1E). BCN1 increased at 48 hours of 100% oxygen compared with normoxia (Figure 1E). Immunohistochemical BCN1 staining in hyperoxia was localized to the epithelium, with particularly marked staining in the airway (Figure 1E). Together, these data indicate that, in lungs of WT mice in 100% oxygen, BCN1 and BCN1 phosphorylation increase at 48 hours. These data also indicate that BCN1 increases in the lung epithelium at 48 hours of hyperoxia.

Hyperoxia induces autophagy in the lung *in vivo*

Based on well-established effects of BCN1 on autophagy, effects of 100% oxygen on autophagy were examined in mouse lungs. WT mice were exposed to 100% oxygen for 24, 48, and 72 hours, and lungs were analyzed for autophagy. To examine autophagy, whole-lung microtubule-associated protein 1B-light chain (LC3B) was evaluated via Western blot (Figure 2A-C). Endogenous LC3B-I is converted into LC3B-II (the phosphatidylethanolamine [PE]-conjugated form), and LC3B-II associates with autophagosome membranes (43). LC3B-II was used to evaluate autophagosome number as LC3B-II levels correlate well with the number of autophagosomes (43). Whole-lung LC3B-II levels were increased at 48 hours of 100% oxygen compared with 24 hours (Figure 2A-B), indicating increased autophagosomes. Whole-lung LC3B-II levels were increased at 48 hours compared with normoxia however this did not reach statistical significance (Figure 2A-B). This indicated increased autophagosome numbers at 48 hours of 100% oxygen. Next, LC3B-II/-I ratios, which are used to evaluate autophagic flux or the level of cellular autophagic activity (43), were assessed via Western blot (Figure

2A, 2C). LC3B-II/-I ratios were decreased at 24 and 72 hours of 100% oxygen compared with normoxia, and LC3B-II/-I ratios were decreased at 48 hours compared with normoxia however this did not reach statistical significance (Figure 2A, 2C). This suggested that autophagic flux was overall decreased at 24 and 72 hours of 100% oxygen compared with normoxia. In addition, whole-lung expression of the autophagy genes autophagy related 5 (ATG5) and LC3B were examined in mouse lungs via RT-qPCR (Figure 2D-E). ATG5 expression increased at 48 hours of 100% oxygen compared with normoxia and 24 hours (Figure 2D). LC3B expression increased at 72 hours of 100% oxygen compared with normoxia, 24 hours, and 48 hours (Figure 2E). There was a trend toward increased LC3B expression 48 hours compared with normoxia, however this did not reach statistical significance (Figure 2E). Together, these data suggest that, in lungs of WT mice in 100% oxygen, autophagosome number and expression of autophagy genes increases at 48 and 72 hours, however autophagic flux decreases at 72 hours. Together with the analyses of BCN1, these data indicate, that in the lung of WT mice in 100% oxygen, BCN1 phosphorylation, BCN1 production, autophagosome number, and autophagy gene expression increase at 48 hours.

EGFR inhibition results in reduced BCN1 phosphorylation in the lung *in vivo* in hyperoxia

We previously showed that Waved-5 ($EGFR^{Wa5/+}$) mice have improved survival and reduced EGFR activation in the lung in 100% oxygen compared with WT (24). $EGFR^{Wa5/+}$ mice contain a point mutation that decreases EGFR activity significantly (34). Based on their improved survival in 100% oxygen and on studies showing regulation of BCN1 by EGFR (33), we hypothesized that phosphorylation of BCN1 was altered in these mice in 100% oxygen compared with WT. Effects of 100% oxygen on BCN1 phosphorylation in the lung were examined in $EGFR^{Wa5/+}$ and WT mice compared with normoxia at 24, 48, and 72 hours. BCN1 (p- [Ser93, -96] and total-fraction) was evaluated via Western blot (Figure 3A-B). In normoxia, there were no differences in total BCN1 and p-/total BCN1 ratios in $EGFR^{Wa5/+}$ mice compared with WT, although total BCN1 levels showed a trend of being increased in $EGFR^{Wa5/+}$ mice and p-/total BCN1 ratios showed a trend of being decreased in $EGFR^{Wa5/+}$ mice (Figure 3A). In 100% oxygen, $EGFR^{Wa5/+}$ mice showed increased total BCN1 and decreased p-/total BCN1 ratios compared with WT (Figure 3B). These data suggest that $EGFR^{Wa5/+}$ mice contain increased total BCN1 and decreased p-/total BCN1 ratios in the lungs in 100% oxygen. In addition, whole-lung expression of BCN1 was evaluated via RT-qPCR. No differences in BCN1 expression were observed between $EGFR^{Wa5/+}$ mice and WT in normoxia (Figure 3C). In 100% oxygen at 24 hours, BCN1 expression increased in $EGFR^{Wa5/+}$ mice compared with WT, however this did not reach statistical significance (Figure 3D). In addition, whole-lung and epithelial-specific BCN1 (p- and total-) were examined in $EGFR^{Wa5/+}$ mice compared with WT using flow cytometry (Figure 4A-E). Mice were exposed to hyperoxia for 48 hours along with normoxia controls. Lungs were isolated, digested into single-cell suspensions, and analyzed with flow cytometry. In WT mice, whole-lung p-/total BCN1 ratios increased at 48 hours of hyperoxia compared with normoxia (Figure 4B). Whole-lung p-/total BCN1 ratios were decreased in $EGFR^{Wa5/+}$ mice compared with WT at 48 hours of hyperoxia, although this did not reach statistical significance (Figure 4C). In WT, epithelial-specific p-/total BCN1 ratios were increased at 48 hours of hyperoxia compared with normoxia, although this did not reach statistical significance (Figure 4D). Epithelial-specific p-/total BCN1 ratios decreased in $EGFR^{Wa5/+}$ mice compared with WT, although this did not reach statistical

significance (Figure 4E). Together, these data suggest that, in 100% oxygen in the lung, EGFR$^{Wa5/+}$ mice have reduced whole-lung and epithelial-specific BCN1 phosphorylation compared with WT.

EGFR inhibition results in decreased autophagy in the lung *in vivo* in hyperoxia

Because BCN1 phosphorylation at Ser93, -96 leads to autophagosome biogenesis (42), we hypothesized that autophagy would be affected in the lungs of EGFR$^{Wa5/+}$ mice compared with WT. Effects of 100% oxygen on whole-lung autophagy were examined in EGFR$^{Wa5/+}$ and WT mice and compared with normoxia. LC3B was assessed via Western blot. LC3B-II/β-Actin ratios, which correlate with autophagosome number, were evaluated. In addition, LCB-II/I ratios, which indicate autophagic flux, were evaluated. No differences were observed in LC3B-II/β-Actin and LCB-II/-I ratios in the lung in EGFR$^{Wa5/+}$ and WT mice in normoxia, although there was a trend toward decreased LC3B-II/β-Actin in EGFR$^{Wa5/+}$ mice compared with WT that did not reach statistical significance (Figure 5A). At 48 hours of 100% oxygen, LC3B-II/β-Actin and LCB-II/-I ratios were both decreased in the lung in EGFR$^{Wa5/+}$ mice compared with WT (Figure 5B). In addition, whole-lung expression of the autophagy gene LC3B was examined in mouse lungs via RT-qPCR. There was a trend toward decreased LC3B expression in EGFR$^{Wa5/+}$ mice compared with WT at 48 hours of hyperoxia, although this did not reach statistical significance (Figure 5C). These data suggest that there is decreased autophagosome number, autophagy activity, and decreased autophagic flux in the lungs of EGFR$^{Wa5/+}$ mice compared with WT in 100% oxygen.

DISCUSSION:

A substantial portion of patients placed on mechanical ventilation in the ICU require hyperoxia to maintain adequate tissue oxygenation. Hyperoxia leads to lung cell death in the airway and alveolar epithelium. In patients with ALI/ARDS who require mechanical ventilation and hyperoxia to maintain proper oxygenation, hyperoxia activates pathways that lead to cell death. Thus, in each individual patient with ARDS exposed to hyperoxia, molecular pathways activated by hyperoxia, ARDS, specific subtypes of ALI (e.g., infectious, thrombotic, chemical, VILI), and countless other processes interact and lead to cell death. Elucidation of mechanisms of cell death in hyperoxia will enable identification of key pathways that are potentially targetable in ALI/ARDS. In addition, hyperoxia is a form of ALI caused by oxidative injury that is a model for ARDS. Despite the high prevalence and substantial mortality for ARDS, there are no medical therapies. In addition, during the COVID-19 pandemic, the number of patients affected with ARDS increased dramatically. Thus, it is critical to identify potential therapeutic targets for ARDS. ARDS is a heterogeneous disease, and further classification of ARDS into distinct subtypes that may or may not respond to specific therapies is an area of active investigation. Because hyperoxia is a form of ARDS that is driven purely by oxidative damage, elucidation of molecular pathways in hyperoxia enables identification of cell death pathways that are active in ARDS mediated by oxidative damage. Thus, therapeutic targets identified in hyperoxia have the potential to be candidate therapeutic targets for ARDS, especially as our ability to identify patient-specific phenotypes in ARDS improves.

This study shows that EGFR regulates BCN1 phosphorylation and autophagy in the lung in hyperoxia. The results show that hyperoxia induces BCN1 phosphorylation in the lung epithelium, increases total BCN1 levels in the lung and in the lung epithelium, and augments specific markers of autophagy in the lung in mice. Inhibition of EGFR reduces BCN1 phosphorylation in the lung epithelium, increases total BCN1 in the lung, and reduces autophagy activity in the lung. Our findings are consistent with previous studies showing increased BCN1 activation and autophagy in hyperoxia (28). In addition, our findings are consistent with well-established EGFR pathways. EGFR activation is known to regulate the mammalian target of rapamycin (mTOR) pathway via phosphoinositide-3-kinase (PI3K)/ v-akt murine thymoma viral oncogene homolog 1 (AKT), and this pathway is known to regulate autophagy (44).

Our study further advances identification of EGFR-mediated cell death pathways in the lung in hyperoxia. The role of BCN1 and autophagy in hyperoxia is not well defined, and the role of BCN1 and autophagy in ALI is an area of active investigation. BCN1 augmentation has been shown to be protective in a sepsis model induced by *Klebsiella pneumoniae* (45). We previously showed that $EGFR^{Wa5/+}$ mice are protected in hyperoxia (24). The augmentation of total BCN1 levels, reduction in BCN1 phosphorylation, and reduced autophagy in the lung in $EGFR^{Wa5/+}$ mice in hyperoxia allows us to speculate that this mechanism plays a role in protection. Decreased BCN1 phosphorylation and subsequent decreased autophagy may reduce cell death mediated by autophagy. This is a potential mechanism in which reduction in BCN1 phosphorylation could be protective in hyperoxia. Whether regulated cell death induced by autophagy, called autophagy-dependent cell death (ADCD) (46, 47), plays a significant role in hyperoxia is not clear and warrants further study. In addition, increased BCN1 levels can bind with and sequester proteins in the BCL2 family and consequently upregulate apoptotic cell death while simultaneously downregulating autophagy, a mechanism which has been shown to be clinically relevant in cardiac disease (48). Effects of EGFR on BCN1 binding to BCL2 family proteins in hyperoxia warrant further study. In addition, the clinical effects of EGFR regulation of BCN1 and autophagy in hyperoxia and the mechanisms that produce these effects warrant further investigation.

LIMITATIONS:

This study has some limitations. First, it remains to be answered whether the reduction in BCN1 activation and decreased autophagy we found in $EGFR^{Wa5/+}$ mice is protective in hyperoxia. We have previously shown that $EGFR^{Wa5/+}$ mice are protected in hyperoxia and have reduced alveolar epithelial cell apoptosis (24). In addition, we previously showed that EGFR inhibition reduces apoptotic cell death in alveolar epithelial cells in hyperoxia. Reduced BCN1 phosphorylation and reduced autophagy in $EGFR^{Wa5/+}$ mice in hyperoxia raises the consideration that this is a protective mechanism, however this requires further study. Studies targeting EGFR-mediated BCN1 activation could help divulge whether this is a protective mechanism in hyperoxia.

Second, to what degree the effects of EGFR on distinct epithelial compartments influence clinical outcomes in hyperoxia remains to be elucidated. Our data indicate that BCN1 increases in the epithelium in hyperoxia, and

there was a particularly marked increase in the airway epithelium. We previously showed effects of EGFR on cell death in the alveolar epithelium. Hyperoxia is known to induce cell death in both airway and alveolar epithelial cells. Together with our prior work, our data suggest that EGFR regulates autophagy and cell death pathways in both airway and alveolar epithelial cellular compartments. How EGFR differentially regulates BCN1 in distinct epithelial compartments in the lung warrants further study but is outside the scope of this manuscript. In addition, to what degree autophagy and cell death in the airway and alveolar epithelial compartments influence the clinical outcome in hyperoxia remains to be elucidated.

CONCLUSIONS:

Exposure to 100% oxygen resulted in increased BCN1 phosphorylation, increased total BCN1, and increased autophagy in the lung. BCN1 phosphorylation increased in epithelial cells. Genetically modified mice with reduced EGFR activity, which are protected in hyperoxia, had decreased BCN1 phosphorylation and reduced autophagy in the lung in hyperoxia.

FIGURE LEGENDS

Figure 1. Hyperoxia leads to increased BCN1 in the lung epithelium *in vivo*. (A-E) Effects of 100% oxygen on BCN1 in the lungs of WT mice at 24, 48, and 72 hours compared with normoxia (*N* = 4-6 mice/group, repeated once). (A) Representative Western blot (WB) on whole lungs for BCN1 (p- and total). (B-C) Quantitative densitometry for (B) p-/total BCN1 and (C) total BCN1/β-Actin is shown. *p < 0.05, **p < 0.005, Mann-Whitney U test. (D) RT-qPCR on whole lungs for BCN1. *p < 0.05, **p < 0.005, ***p < 0.0005, Mann-Whitney U test. (E) IHC on lungs for BCN1 at 48 hours compared with normoxia, scale bar = 100 µm. Quantification of H-score is shown. *p < 0.05, unpaired t test. BCN1, Beclin-1.

Figure 2. Hyperoxia induces autophagy in the lung *in vivo*. (A-E) Effects of 100% oxygen on autophagy in the lungs of WT mice at 24, 48, and 72 hours compared with normoxia (*N* = 4-6 mice/group, repeated once). (A) Representative WB on whole lungs for LC3B. (B-C) Quantitative densitometry for (B) LC3B-II/β-Actin and (C) LC3B-II/-I is shown. *p < 0.05, Mann-Whitney U test. (D-E) RT-qPCR on whole lungs for (D) ATG5 and (E) LC3B. *p < 0.05, **p < 0.005, ***p < 0.0005, ****p < 0.0001, Mann-Whitney U test. ATG5, autophagy related 5. LC3B, microtubule-associated protein 1B-light chain.

Figure 3. EGFR inhibition results in increased BCN1 and reduced BCN1 activation in the lung in hyperoxia *in vivo*. (A-D) Effects of 100% oxygen on BCN1 in the lungs of $EGFR^{Wa5/+}$ and WT mice compared with normoxia (*N* = 4-6 mice/group, repeated twice). (A-B) Representative WB for BCN1 (p- and total) on whole lungs with quantitative densitometry for total BCN1/β-Actin and p-/total BCN1. (A) Normoxia. (B) 100% oxygen, 48 hours. **p < 0.005, Mann-Whitney U test. (C-D) RT-qPCR for BCN1 on whole lungs. (C) Normoxia. (D) 100% oxygen, 48 hours. BCN1, Beclin-1. Wa5, $EGFR^{Wa5/+}$.

Figure 4. BCN1 is activated by hyperoxia in lung epithelium and is regulated by EGFR. (A-E) Effects of 100% oxygen on BCN1 (p- and total) via flow cytometry in the lungs of $EGFR^{Wa5/+}$ and WT mice compared with normoxia (*N* = 4-6 mice/group). (A) Gating strategy to isolate epithelial-specific BCN1 (p- and total). (B-E) The ratio of percentage of positive cells for p-/total BCN1 is shown for (B-C) all lung cells and (D-E) epithelial lung cells. (B) WT, all lung cells, normoxia vs. 48 hours of 100% oxygen; (C) WT vs. $EGFR^{Wa5/+}$, all lung cells, 48 hours of 100% oxygen; (D) WT, epithelial cells, normoxia vs. 48 hours of 100% oxygen; (E) WT vs. $EGFR^{Wa5/+}$, epithelial cells, 48 hours of 100% oxygen. *p < 0.05, unpaired t test. BCN1, Beclin-1. Wa5, $EGFR^{Wa5/+}$.

Figure 5. EGFR inhibition leads to reduced autophagy in hyperoxia. (A-C) Effects of 100% oxygen on autophagy in the lungs of $EGFR^{Wa5/+}$ and WT mice compared with normoxia (*N* = 4-6 mice/group, repeated twice). (A-B) Representative WB on whole lungs for LC3B with quantitative densitometry for LC3B-II/β-Actin and LC3B-II/-I. (A) Normoxia. (B) 100% oxygen, 48 hours. *p < 0.05, Mann-Whitney U test. (C) RT-qPCR for BCN1 on whole lungs for LC3B. LC3B, microtubule-associated protein 1B-light chain. Wa5, $EGFR^{Wa5/+}$.

Supplemental Figure S1A. Hyperoxia leads to increased BCN1 in the lung epithelium *in vivo*. Effects of 100% oxygen on BCN1 in the lungs of WT mice at 24, 48, and 72 hours compared with normoxia (*N* = 4-6 mice/group, repeated once). RT-qPCR on whole lungs for BCN1. **$p < 0.005$, ***$p < 0.0005$, Mann-Whitney U test. BCN1, Beclin-1.

REFERENCES

1. Behrendt CE. Acute respiratory failure in the United States: incidence and 31-day survival. Chest. 2000;118(4):1100-5. Epub 2000/10/18. doi: 10.1378/chest.118.4.1100. PubMed PMID: 11035684.

2. Kahn JM, Goss CH, Heagerty PJ, Kramer AA, O'Brien CR, Rubenfeld GD. Hospital volume and the outcomes of mechanical ventilation. N Engl J Med. 2006;355(1):41-50. Epub 2006/07/11. doi: 10.1056/NEJMsa053993. PubMed PMID: 16822995.

3. Wunsch H, Linde-Zwirble WT, Angus DC, Hartman ME, Milbrandt EB, Kahn JM. The epidemiology of mechanical ventilation use in the United States. Crit Care Med. 2010;38(10):1947-53. Epub 2010/07/20. doi: 10.1097/CCM.0b013e3181ef4460. PubMed PMID: 20639743.

4. Bellani G, Laffey JG, Pham T, Fan E, Brochard L, Esteban A, Gattinoni L, van Haren F, Larsson A, McAuley DF, Ranieri M, Rubenfeld G, Thompson BT, Wrigge H, Slutsky AS, Pesenti A, Investigators LS, Group ET. Epidemiology, Patterns of Care, and Mortality for Patients With Acute Respiratory Distress Syndrome in Intensive Care Units in 50 Countries. JAMA. 2016;315(8):788-800. Epub 2016/02/24. doi: 10.1001/jama.2016.0291. PubMed PMID: 26903337.

5. Grasselli G, Zangrillo A, Zanella A, Antonelli M, Cabrini L, Castelli A, Cereda D, Coluccello A, Foti G, Fumagalli R, Iotti G, Latronico N, Lorini L, Merler S, Natalini G, Piatti A, Ranieri MV, Scandroglio AM, Storti E, Cecconi M, Pesenti A, Network C-LI. Baseline Characteristics and Outcomes of 1591 Patients Infected With SARS-CoV-2 Admitted to ICUs of the Lombardy Region, Italy. JAMA. 2020;323(16):1574-81. Epub 2020/04/07. doi: 10.1001/jama.2020.5394. PubMed PMID: 32250385; PMCID: PMC7136855.

6. Budinger GR, Mutlu GM, Urich D, Soberanes S, Buccellato LJ, Hawkins K, Chiarella SE, Radigan KA, Eisenbart J, Agrawal H, Berkelhamer S, Hekimi S, Zhang J, Perlman H, Schumacker PT, Jain M, Chandel NS. Epithelial cell death is an important contributor to oxidant-mediated acute lung injury. Am J Respir Crit Care Med. 2011;183(8):1043-54. Epub 2010/10/21. doi: 10.1164/rccm.201002-0181OC. PubMed PMID: 20959557; PMCID: PMC3086743.

7. Rubenfeld GD, Caldwell E, Peabody E, Weaver J, Martin DP, Neff M, Stern EJ, Hudson LD. Incidence and outcomes of acute lung injury. N Engl J Med. 2005;353(16):1685-93. Epub 2005/10/21. doi: 10.1056/NEJMoa050333. PubMed PMID: 16236739.

8. Finigan JH, Downey GP, Kern JA. Human epidermal growth factor receptor signaling in acute lung injury. Am J Respir Cell Mol Biol. 2012;47(4):395-404. Epub 2012/06/02. doi: 10.1165/rcmb.2012-0100TR. PubMed PMID: 22652197; PMCID: PMC3488630.

9. Leslie CC, McCormick-Shannon K, Shannon JM, Garrick B, Damm D, Abraham JA, Mason RJ. Heparin-binding EGF-like growth factor is a mitogen for rat alveolar type II cells. Am J Respir Cell Mol Biol. 1997;16(4):379-87. Epub 1997/04/01. doi: 10.1165/ajrcmb.16.4.9115748. PubMed PMID: 9115748.

10. Dlugosz AA, Cheng C, Denning MF, Dempsey PJ, Coffey RJ, Jr., Yuspa SH. Keratinocyte growth factor receptor ligands induce transforming growth factor alpha expression and activate the epidermal growth factor receptor signaling pathway in cultured epidermal keratinocytes. Cell Growth Differ. 1994;5(12):1283-92. Epub 1994/12/01. PubMed PMID: 7535082.

11. Kheradmand F, Folkesson HG, Shum L, Derynk R, Pytela R, Matthay MA. Transforming growth factor-alpha enhances alveolar epithelial cell repair in a new in vitro model. Am J Physiol. 1994;267(6 Pt 1):L728-38. Epub 1994/12/01. doi: 10.1152/ajplung.1994.267.6.L728. PubMed PMID: 7810677.
12. Crosby LM, Waters CM. Epithelial repair mechanisms in the lung. Am J Physiol Lung Cell Mol Physiol. 2010;298(6):L715-31. Epub 2010/04/07. doi: 10.1152/ajplung.00361.2009. PubMed PMID: 20363851; PMCID: PMC2886606.
13. Koff JL, Shao MX, Kim S, Ueki IF, Nadel JA. Pseudomonas lipopolysaccharide accelerates wound repair via activation of a novel epithelial cell signaling cascade. J Immunol. 2006;177(12):8693-700. Epub 2006/12/05. doi: 10.4049/jimmunol.177.12.8693. PubMed PMID: 17142770.
14. Gorissen SH, Hristova M, Habibovic A, Sipsey LM, Spiess PC, Janssen-Heininger YM, van der Vliet A. Dual oxidase-1 is required for airway epithelial cell migration and bronchiolar reepithelialization after injury. Am J Respir Cell Mol Biol. 2013;48(3):337-45. Epub 2012/12/15. doi: 10.1165/rcmb.2012-0393OC. PubMed PMID: 23239498; PMCID: PMC3604089.
15. Harada C, Kawaguchi T, Ogata-Suetsugu S, Yamada M, Hamada N, Maeyama T, Souzaki R, Tajiri T, Taguchi T, Kuwano K, Nakanishi Y. EGFR tyrosine kinase inhibition worsens acute lung injury in mice with repairing airway epithelium. Am J Respir Crit Care Med. 2011;183(6):743-51. Epub 2010/10/12. doi: 10.1164/rccm.201002-0188OC. PubMed PMID: 20935109.
16. Bierman A, Yerrapureddy A, Reddy NM, Hassoun PM, Reddy SP. Epidermal growth factor receptor (EGFR) regulates mechanical ventilation-induced lung injury in mice. Transl Res. 2008;152(6):265-72. Epub 2008/12/09. doi: 10.1016/j.trsl.2008.10.004. PubMed PMID: 19059161; PMCID: PMC2646043.
17. Tao H, Li N, Zhang Z, Mu H, Meng C, Xia H, Fu L, Xu Y, Zhang S. Erlotinib Protects LPS-Induced Acute Lung Injury in Mice by Inhibiting EGFR/TLR4 Signaling Pathway. Shock. 2019;51(1):131-8. Epub 2018/02/14. doi: 10.1097/SHK.0000000000001124. PubMed PMID: 29438224.
18. Le Cras TD, Acciani TH, Mushaben EM, Kramer EL, Pastura PA, Hardie WD, Korfhagen TR, Sivaprasad U, Ericksen M, Gibson AM, Holtzman MJ, Whitsett JA, Hershey GK. Epithelial EGF receptor signaling mediates airway hyperreactivity and remodeling in a mouse model of chronic asthma. Am J Physiol Lung Cell Mol Physiol. 2011;300(3):L414-21. Epub 2011/01/13. doi: 10.1152/ajplung.00346.2010. PubMed PMID: 21224214; PMCID: PMC3064289.
19. Hardie WD, Davidson C, Ikegami M, Leikauf GD, Le Cras TD, Prestridge A, Whitsett JA, Korfhagen TR. EGF receptor tyrosine kinase inhibitors diminish transforming growth factor-alpha-induced pulmonary fibrosis. Am J Physiol Lung Cell Mol Physiol. 2008;294(6):L1217-25. Epub 2008/04/22. doi: 10.1152/ajplung.00020.2008. PubMed PMID: 18424623.
20. Ishii Y, Fujimoto S, Fukuda T. Gefitinib prevents bleomycin-induced lung fibrosis in mice. Am J Respir Crit Care Med. 2006;174(5):550-6. Epub 2006/06/03. doi: 10.1164/rccm.200509-1534OC. PubMed PMID: 16741154.
21. Kalinowski A, Galen BT, Ueki IF, Sun Y, Mulenos A, Osafo-Addo A, Clark B, Joerns J, Liu W, Nadel JA, Dela Cruz CS, Koff JL. Respiratory syncytial virus activates epidermal growth factor receptor to suppress interferon regulatory factor 1-dependent interferon-lambda and antiviral defense in airway epithelium. Mucosal

Immunol. 2018;11(3):958-67. Epub 2018/02/08. doi: 10.1038/mi.2017.120. PubMed PMID: 29411775; PMCID: PMC6431552.
22. Kalinowski A, Ueki I, Min-Oo G, Ballon-Landa E, Knoff D, Galen B, Lanier LL, Nadel JA, Koff JL. EGFR activation suppresses respiratory virus-induced IRF1-dependent CXCL10 production. Am J Physiol Lung Cell Mol Physiol. 2014;307(2):L186-96. Epub 2014/05/20. doi: 10.1152/ajplung.00368.2013. PubMed PMID: 24838750; PMCID: PMC4101792.
23. Ueki IF, Min-Oo G, Kalinowski A, Ballon-Landa E, Lanier LL, Nadel JA, Koff JL. Respiratory virus-induced EGFR activation suppresses IRF1-dependent interferon lambda and antiviral defense in airway epithelium. J Exp Med. 2013;210(10):1929-36. Epub 2013/09/04. doi: 10.1084/jem.20121401. PubMed PMID: 23999497; PMCID: PMC3782052.
24. Harris ZM, Sun Y, Joerns J, Clark B, Hu B, Korde A, Sharma L, Shin HJ, Manning EP, Placek L, Unutmaz D, Stanley G, Chun H, Sauler M, Rajagopalan G, Zhang X, Kang MJ, Koff JL. Epidermal Growth Factor Receptor Inhibition Is Protective in Hyperoxia-Induced Lung Injury. Oxid Med Cell Longev. 2022;2022:9518592. Epub 2022/10/05. doi: 10.1155/2022/9518592. PubMed PMID: 36193076; PMCID: PMC9526641 publication of this article.
25. Choi AM, Ryter SW, Levine B. Autophagy in human health and disease. N Engl J Med. 2013;368(7):651-62. Epub 2013/02/15. doi: 10.1056/NEJMra1205406. PubMed PMID: 23406030.
26. Shibutani ST, Yoshimori T. A current perspective of autophagosome biogenesis. Cell Res. 2014;24(1):58-68. Epub 2013/12/04. doi: 10.1038/cr.2013.159. PubMed PMID: 24296784; PMCID: PMC3879706.
27. Levy JMM, Towers CG, Thorburn A. Targeting autophagy in cancer. Nat Rev Cancer. 2017;17(9):528-42. Epub 2017/07/29. doi: 10.1038/nrc.2017.53. PubMed PMID: 28751651; PMCID: PMC5975367.
28. Tanaka A, Jin Y, Lee SJ, Zhang M, Kim HP, Stolz DB, Ryter SW, Choi AM. Hyperoxia-induced LC3B interacts with the Fas apoptotic pathway in epithelial cell death. Am J Respir Cell Mol Biol. 2012;46(4):507-14. Epub 2011/11/19. doi: 10.1165/rcmb.2009-0415OC. PubMed PMID: 22095627; PMCID: PMC3359946.
29. Kaufmann T, Strasser A, Jost PJ. Fas death receptor signalling: roles of Bid and XIAP. Cell Death Differ. 2012;19(1):42-50. Epub 2011/10/01. doi: 10.1038/cdd.2011.121. PubMed PMID: 21959933; PMCID: PMC3252833.
30. Menon MB, Dhamija S. Beclin 1 Phosphorylation - at the Center of Autophagy Regulation. Front Cell Dev Biol. 2018;6:137. Epub 2018/10/30. doi: 10.3389/fcell.2018.00137. PubMed PMID: 30370269; PMCID: PMC6194997.
31. Han J, Hou W, Lu C, Goldstein LA, Stolz DB, Watkins SC, Rabinowich H. Interaction between Her2 and Beclin-1 proteins underlies a new mechanism of reciprocal regulation. J Biol Chem. 2013;288(28):20315-25. Epub 2013/05/25. doi: 10.1074/jbc.M113.461350. PubMed PMID: 23703612; PMCID: PMC3711298.
32. Tan X, Lambert PF, Rapraeger AC, Anderson RA. Stress-Induced EGFR Trafficking: Mechanisms, Functions, and Therapeutic Implications. Trends Cell Biol. 2016;26(5):352-66. Epub 2016/02/02. doi: 10.1016/j.tcb.2015.12.006. PubMed PMID: 26827089; PMCID: PMC5120732.

33. Wei Y, Zou Z, Becker N, Anderson M, Sumpter R, Xiao G, Kinch L, Koduru P, Christudass CS, Veltri RW, Grishin NV, Peyton M, Minna J, Bhagat G, Levine B. EGFR-mediated Beclin 1 phosphorylation in autophagy suppression, tumor progression, and tumor chemoresistance. Cell. 2013;154(6):1269-84. Epub 2013/09/17. doi: 10.1016/j.cell.2013.08.015. PubMed PMID: 24034250; PMCID: PMC3917713.
34. Lee D, Cross SH, Strunk KE, Morgan JE, Bailey CL, Jackson IJ, Threadgill DW. Wa5 is a novel ENU-induced antimorphic allele of the epidermal growth factor receptor. Mamm Genome. 2004;15(7):525-36. Epub 2004/09/16. doi: 10.1007/s00335-004-2384-2. PubMed PMID: 15366372.
35. Zhang Y, Jiang G, Sauler M, Lee PJ. Lung endothelial HO-1 targeting in vivo using lentiviral miRNA regulates apoptosis and autophagy during oxidant injury. FASEB J. 2013;27(10):4041-58. Epub 2013/06/19. doi: 10.1096/fj.13-231225. PubMed PMID: 23771928; PMCID: PMC4046184.
36. Sauler M, Zhang Y, Min JN, Leng L, Shan P, Roberts S, Jorgensen WL, Bucala R, Lee PJ. Endothelial CD74 mediates macrophage migration inhibitory factor protection in hyperoxic lung injury. FASEB J. 2015;29(5):1940-9. Epub 2015/01/23. doi: 10.1096/fj.14-260299. PubMed PMID: 25609432; PMCID: PMC4415022.
37. Kim HR, Kim MN, Kim EG, Leem JS, Baek SM, Lee YJ, Kim KW, Kang MJ, Song TW, Sohn MH. NLRX1 knockdown attenuates pro-apoptotic signaling and cell death in pulmonary hyperoxic acute injury. Sci Rep. 2023;13(1):3441. Epub 2023/03/02. doi: 10.1038/s41598-023-28206-x. PubMed PMID: 36859435; PMCID: PMC9975446.
38. Pua HH, Dzhagalov I, Chuck M, Mizushima N, He YW. A critical role for the autophagy gene Atg5 in T cell survival and proliferation. J Exp Med. 2007;204(1):25-31. Epub 2006/12/28. doi: 10.1084/jem.20061303. PubMed PMID: 17190837; PMCID: PMC2118420.
39. Gawriluk TR, Ko C, Hong X, Christenson LK, Rucker EB, 3rd. Beclin-1 deficiency in the murine ovary results in the reduction of progesterone production to promote preterm labor. Proc Natl Acad Sci U S A. 2014;111(40):E4194-203. Epub 2014/09/24. doi: 10.1073/pnas.1409323111. PubMed PMID: 25246579; PMCID: PMC4210046.
40. Komatsu M, Waguri S, Ueno T, Iwata J, Murata S, Tanida I, Ezaki J, Mizushima N, Ohsumi Y, Uchiyama Y, Kominami E, Tanaka K, Chiba T. Impairment of starvation-induced and constitutive autophagy in Atg7-deficient mice. J Cell Biol. 2005;169(3):425-34. Epub 2005/05/04. doi: 10.1083/jcb.200412022. PubMed PMID: 15866887; PMCID: PMC2171928.
41. Fedchenko N, Reifenrath J. Different approaches for interpretation and reporting of immunohistochemistry analysis results in the bone tissue - a review. Diagn Pathol. 2014;9:221. Epub 2014/11/30. doi: 10.1186/s13000-014-0221-9. PubMed PMID: 25432701; PMCID: PMC4260254.
42. Kim J, Kim YC, Fang C, Russell RC, Kim JH, Fan W, Liu R, Zhong Q, Guan KL. Differential regulation of distinct Vps34 complexes by AMPK in nutrient stress and autophagy. Cell. 2013;152(1-2):290-303. Epub 2013/01/22. doi: 10.1016/j.cell.2012.12.016. PubMed PMID: 23332761; PMCID: PMC3587159.
43. Mizushima N, Yoshimori T, Levine B. Methods in mammalian autophagy research. Cell. 2010;140(3):313-26. Epub 2010/02/11. doi: 10.1016/j.cell.2010.01.028. PubMed PMID: 20144757; PMCID: PMC2852113.

44. Jutten B, Rouschop KM. EGFR signaling and autophagy dependence for growth, survival, and therapy resistance. Cell Cycle. 2014;13(1):42-51. Epub 2013/12/18. doi: 10.4161/cc.27518. PubMed PMID: 24335351; PMCID: PMC3925733.
45. Nikouee A, Kim M, Ding X, Sun Y, Zang QS. Beclin-1-Dependent Autophagy Improves Outcomes of Pneumonia-Induced Sepsis. Front Cell Infect Microbiol. 2021;11:706637. Epub 2021/07/03. doi: 10.3389/fcimb.2021.706637. PubMed PMID: 34211859; PMCID: PMC8239405.
46. Jung S, Jeong H, Yu SW. Autophagy as a decisive process for cell death. Exp Mol Med. 2020;52(6):921-30. Epub 2020/06/28. doi: 10.1038/s12276-020-0455-4. PubMed PMID: 32591647; PMCID: PMC7338414.
47. Liu S, Yao S, Yang H, Liu S, Wang Y. Autophagy: Regulator of cell death. Cell Death Dis. 2023;14(10):648. Epub 2023/10/05. doi: 10.1038/s41419-023-06154-8. PubMed PMID: 37794028; PMCID: PMC10551038.
48. Maejima Y, Kyoi S, Zhai P, Liu T, Li H, Ivessa A, Sciarretta S, Del Re DP, Zablocki DK, Hsu CP, Lim DS, Isobe M, Sadoshima J. Mst1 inhibits autophagy by promoting the interaction between Beclin1 and Bcl-2. Nat Med. 2013;19(11):1478-88. Epub 2013/10/22. doi: 10.1038/nm.3322. PubMed PMID: 24141421; PMCID: PMC3823824.

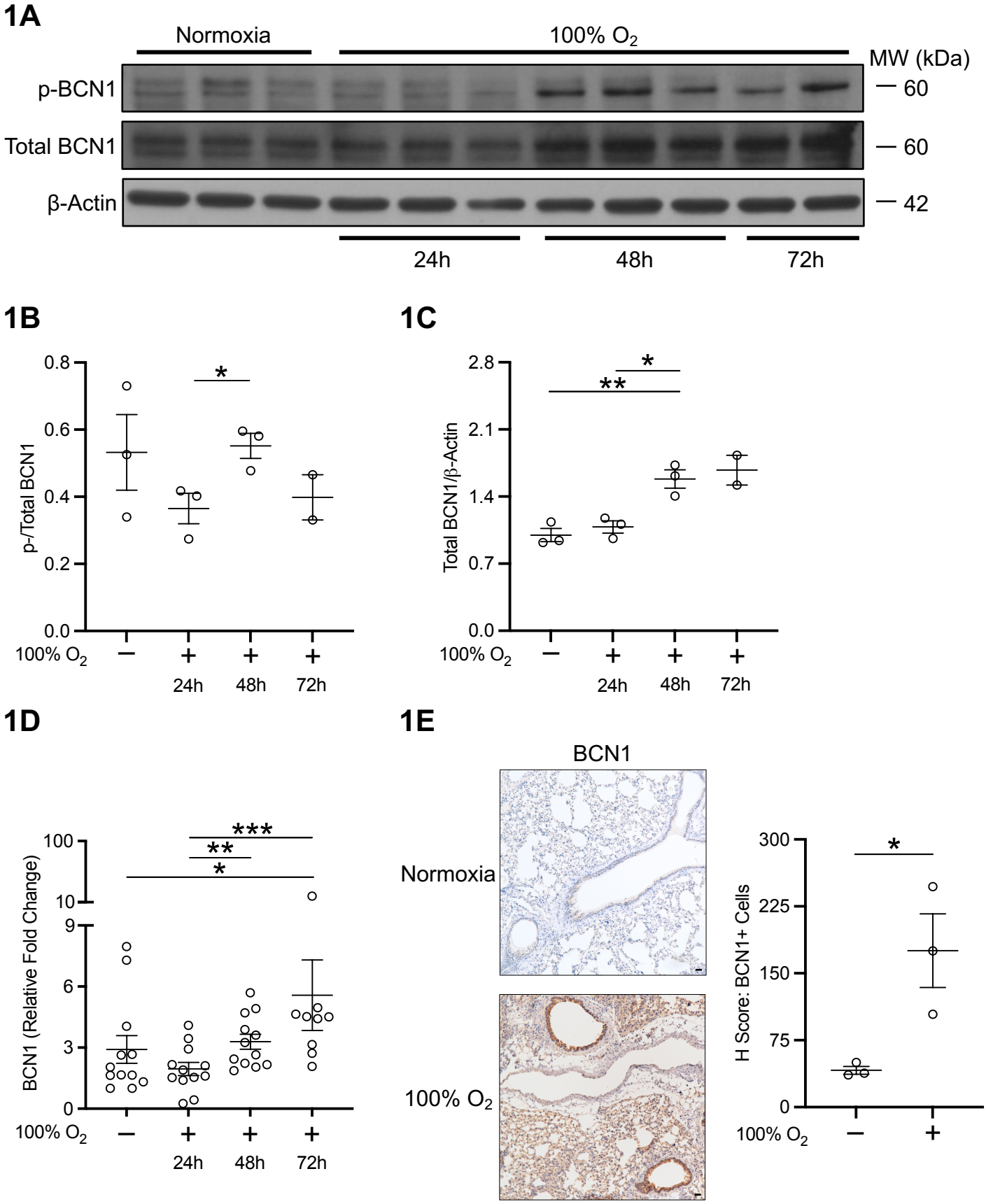
1A
Normoxia
100% O2
MW (kDa)
p-BCN1
Total BCN1
β-Actin
60
60
42
24h
48h
72h
1B
p-/Total BCN1
0.8
0.6
0.4
0.2
0.0
*
100% O2
−
+
+
+
24h
48h
72h
1C
Total BCN1/β-Actin
2.8
2.1
1.4
0.7
0.0
*
**
100% O2
−
+
+
+
24h
48h
72h
1D
BCN1 (Relative Fold Change)
100
10
9
6
3
0
***
**
*
100% O2
−
+
+
+
24h
48h
72h
1E
BCN1
Normoxia
100% O2
H Score: BCN1+ Cells
300
225
150
75
0
*
100% O2
−
+

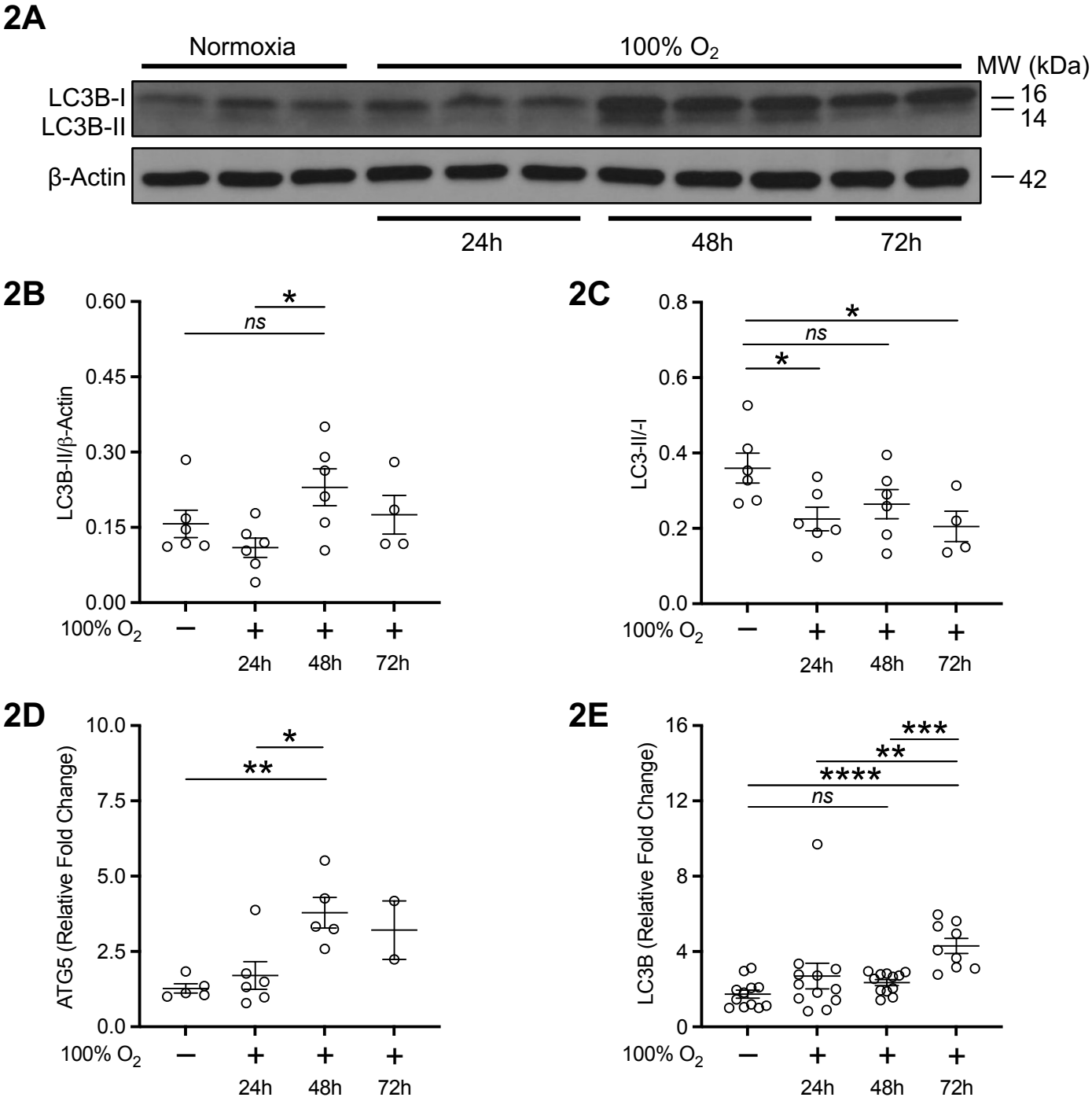
2A
Normoxia
100% O2
MW (kDa)
LC3B-I
LC3B-II
16
14
β-Actin
42
24h
48h
72h
2B
LC3B-II/β-Actin
0.60
0.45
0.30
0.15
0.00
*
ns
100% O2
−
+
+
+
24h
48h
72h
2C
LC3-II/-I
0.8
0.6
0.4
0.2
0.0
*
ns
*
100% O2
−
+
+
+
24h
48h
72h
2D
ATG5 (Relative Fold Change)
10.0
7.5
5.0
2.5
0.0
*
**
100% O2
−
+
+
+
24h
48h
72h
2E
LC3B (Relative Fold Change)
16
12
8
4
0
***
**
****
ns
100% O2
−
+
+
+
24h
48h
72h

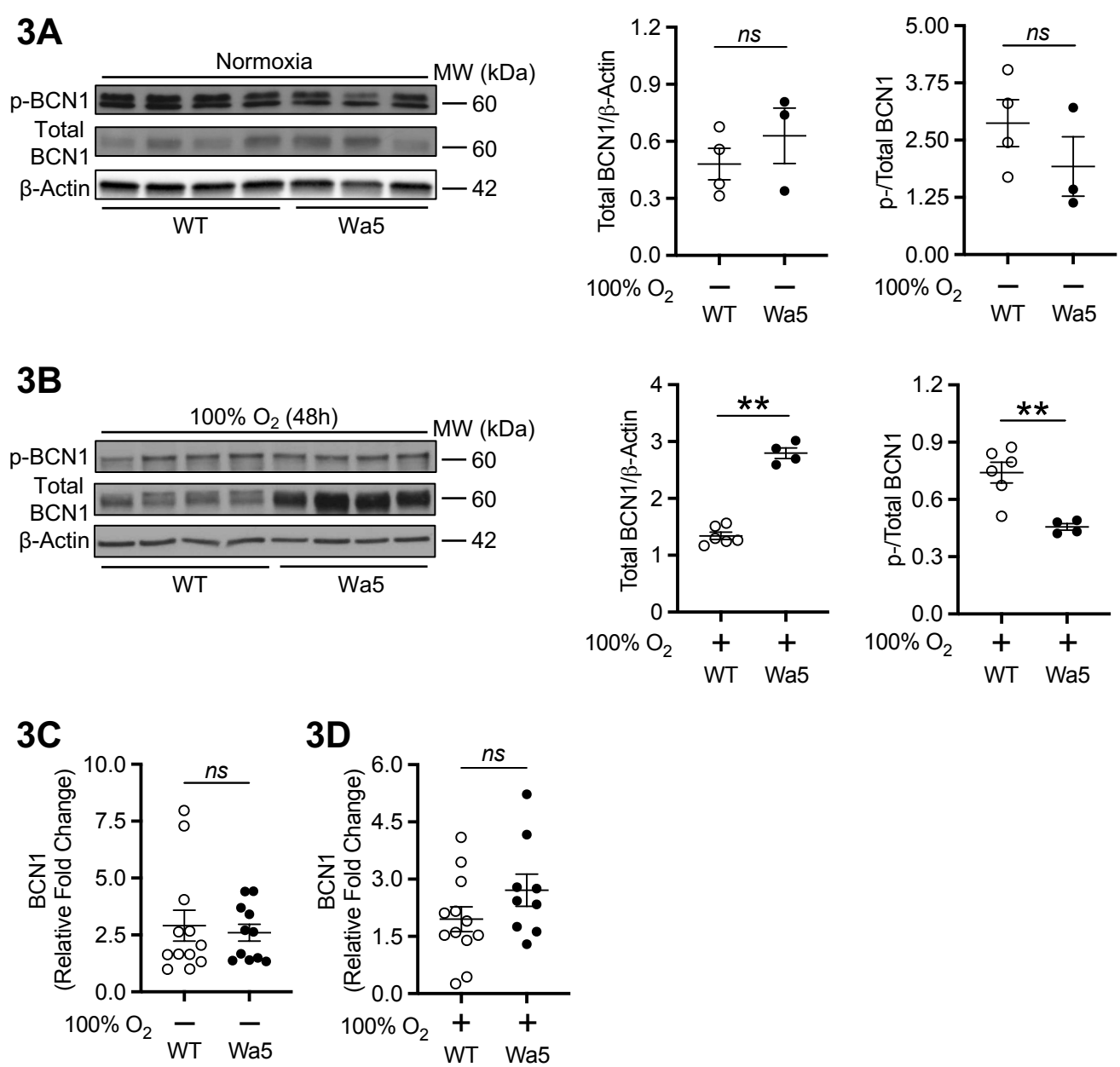
3A
Normoxia
MW (kDa)
p-BCN1
Total BCN1
β-Actin
60
60
42
WT
Wa5
Total BCN1/β-Actin
ns
p-/Total BCN1
100% O2
3B
100% O2 (48h)
**
3C
BCN1 (Relative Fold Change)
3D

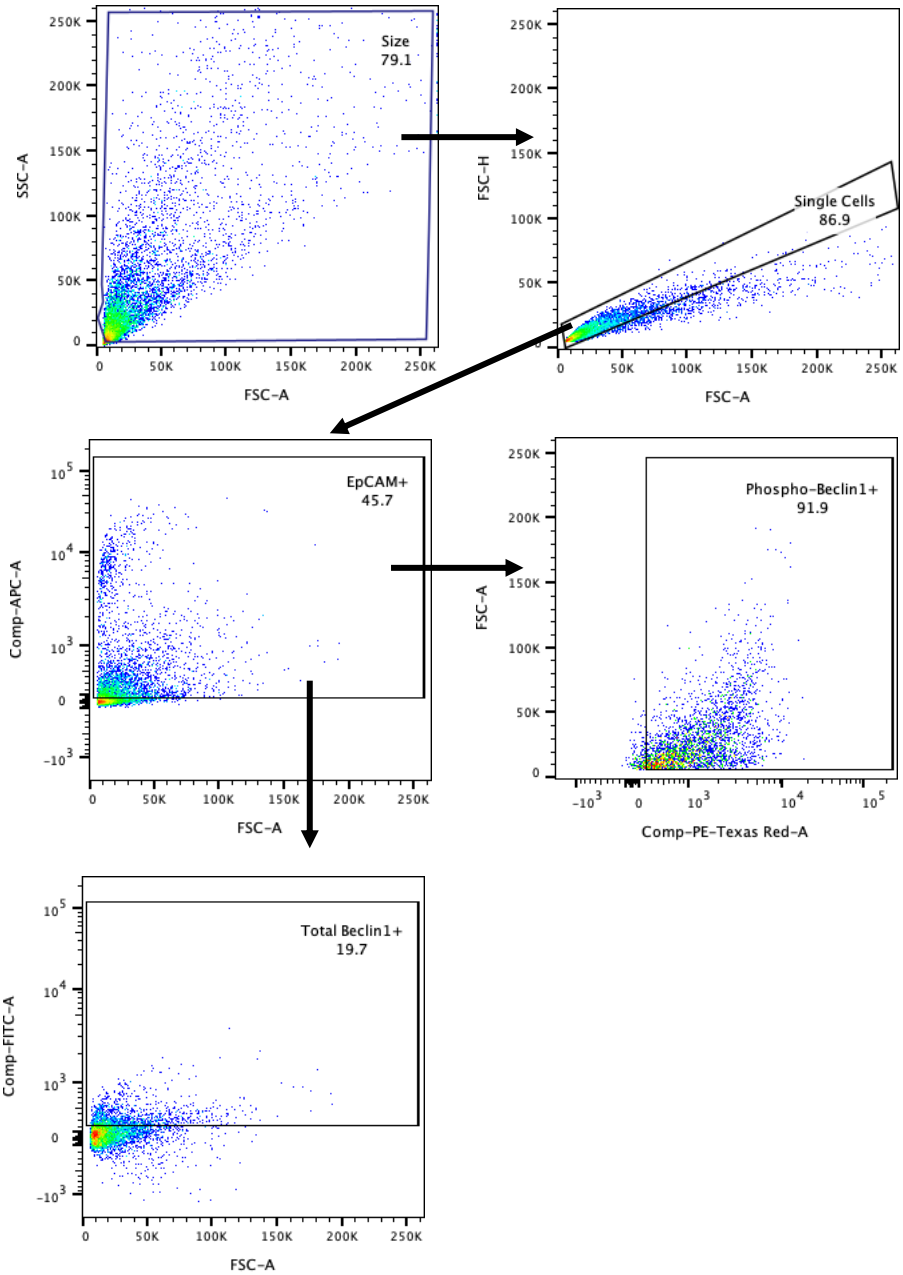
4A
Size
79.1
SSC-A
FSC-A
Single Cells
86.9
FSC-H
FSC-A
EpCAM+
45.7
Comp-APC-A
FSC-A
Phospho-Beclin1+
91.9
FSC-A
Comp-PE-Texas Red-A
Total Beclin1+
19.7
Comp-FITC-A
FSC-A

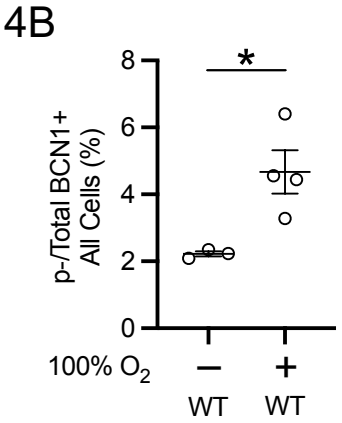
4B
*
p-/Total BCN1+
All Cells (%)
100% O2
–
+
WT
WT

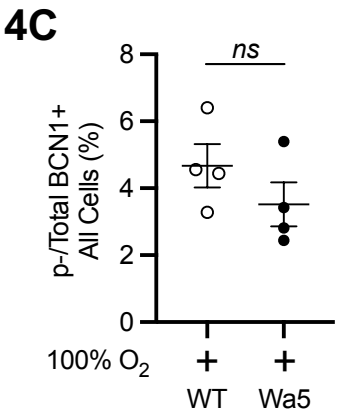
4C
ns
p-/Total BCN1+
All Cells (%)
100% O2
+
+
WT
Wa5

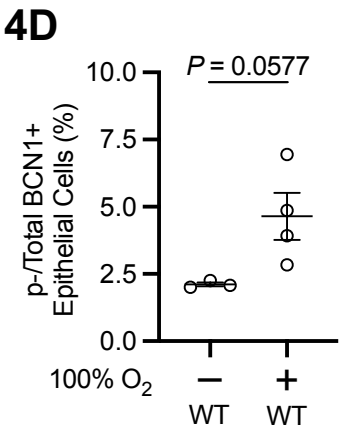
4D
P = 0.0577
p-/Total BCN1+
Epithelial Cells (%)
100% O2
–
+
WT
WT

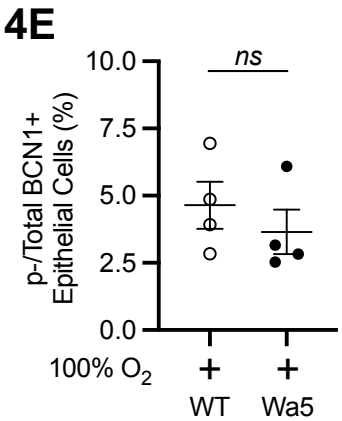
4E
ns
p-/Total BCN1+
Epithelial Cells (%)
100% O2
+
+
WT
Wa5

5A

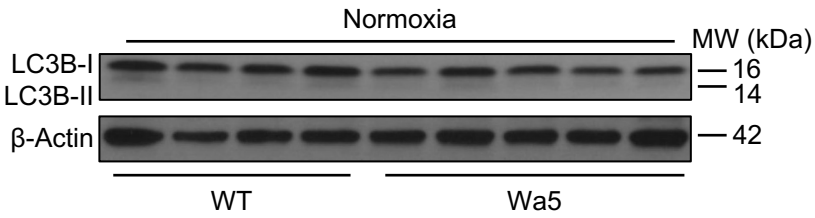
Normoxia
MW (kDa)
LC3B-I
LC3B-II
β-Actin
16
14
42
WT
Wa5

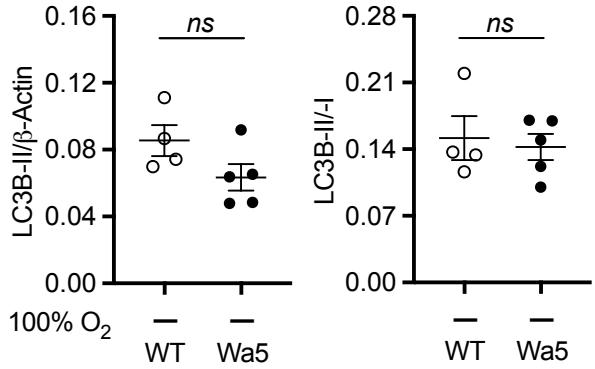
ns
LC3B-II/β-Actin
0.16
0.12
0.08
0.04
0.00
100% O2
WT
Wa5
ns
LC3B-II/-I
0.28
0.21
0.14
0.07
0.00
WT
Wa5

5B

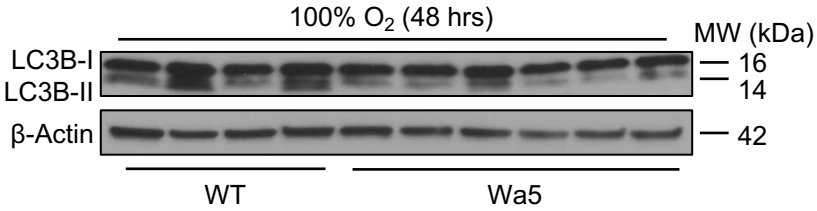
100% O2 (48 hrs)
MW (kDa)
LC3B-I
LC3B-II
β-Actin
16
14
42
WT
Wa5

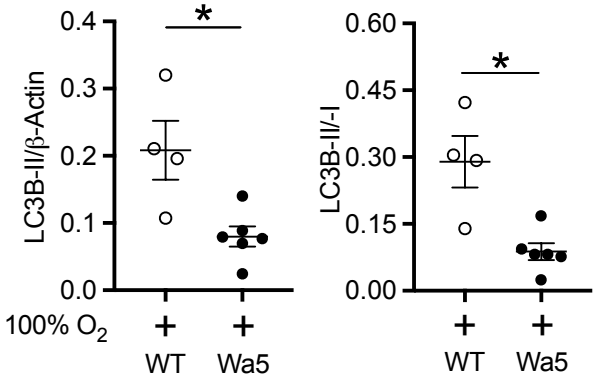
*
LC3B-II/β-Actin
0.4
0.3
0.2
0.1
0.0
100% O2
WT
Wa5
*
LC3B-II/-I
0.60
0.45
0.30
0.15
0.00
WT
Wa5

5C

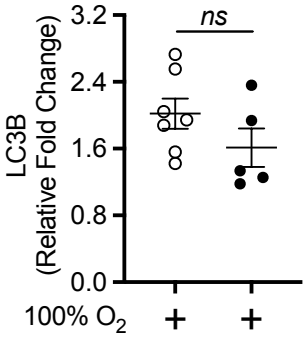
ns
LC3B
(Relative Fold Change)
3.2
2.4
1.6
0.8
0.0
100% O2